Journal of Solid State Chemistry 184 (2011) 191–198

Contents lists available at ScienceDirect

Journal of Solid State Chemistry

journal homepage: www.elsevier.com/locate/jssc

$Cu_{22}Bi_{12}S_{21}Cl_{16}$—A mixed conductor with fast one-dimensional copper(I) ion transport

Andreas Heerwig [a], Rotraut Merkle [b], Joachim Maier [b], Michael Ruck [a,*]

[a] Department of Chemistry and Food Chemistry, Dresden University of Technology, 01062 Dresden, Germany
[b] Max Planck Institute for Solid State Research, Heisenbergstr. 1, 70569 Stuttgart, Germany

ARTICLE INFO

Article history:
Received 17 September 2010
Received in revised form
27 October 2010
Accepted 31 October 2010
Available online 5 November 2010

Keywords:
Bismuth
Copper
Covalent polyhedra networks
Ion conductivity
Thermoelectrics

ABSTRACT

Melting reactions of Cu, CuCl, S, and Bi_2S_3 yield black, shiny needles of $Cu_{22(1)}Bi_{12}S_{21(1)}Cl_{16(1)}$. The compound decomposes peritectically at 649(5) K. Oxidation state +I of the copper atoms is supported by Cu–*K*-XANES. The compound crystallizes in the hexagonal space group $P6/m$ with $a=2116.7(7)$ pm and $c=395.17(5)$ pm. Seven anions coordinate each of the two independent bismuth cations in the shape of mono-capped trigonal prisms. These polyhedra share edges and faces to form trigonal and hexagonal tubes running along [0 0 1]. The hexagonal tubes are centered by chloride ions, which are surrounded by disordered copper cations. The majority of copper cations are distributed over numerous sites between the tubes. The Joint Probability Density Function (JPDF) reveals a continuous pathway along [0 0 1]. The high mobility of the copper cations along [0 0 1] was demonstrated by impedance spectroscopy and DC polarization measurements on single crystals. The ionic conductivity at 450 K is about $\sigma_{ion}=0.06$ S cm^{-1}, and the activation energy for Cu^+ ion conduction is $E_a=0.44$ eV. The chemical diffusion coefficient of copper is in the order of $D^{\delta}_{Cu}=10^{19}$ cm^{-3} at 420 K. The electronic band gap (p-type conductor) was determined as $E_g=0.06$ eV. At room temperature the thermal conductivity of a pressed pellet is about $\kappa=0.3$ W K^{-1} m^{-1} and the Seebeck coefficient is $S=43$ μV K^{-1}.

1. Introduction

Quaternary compounds of the systems Cu/Bi/*Q*/*X* (*Q*=S, Se; *X*=Cl, Br, I) typically consist of rigid networks, which are formed by chalcogenide halide polyhedra around the bismuth(III) cations, and copper(I) cations, which are spread over numerous contiguous voids in between [1,2]. Two physical phenomena can arise from the disorder of copper cations: On the one hand, the migration of copper ions through the crystal can be rather facile resulting in high ion conductivity. $Cu_9Bi_9S_{16}Cl_8$ [1] and $Cu_7Bi_6S_{10}Cl_5$ [2], for instance, exhibit continuous pathways for copper ion diffusion, which can be visualized by the Joint Probability Density Function (JPDF). On the other hand – and this might be more promising – the combination of massive structural disorder, heavy atoms, small band gaps, and a complex band structure around the Fermi level appears to be a good recipe for thermoelectric materials. For the chemically and structurally related compound $K_2Bi_8Se_{13}$ a figure of merit $ZT=0.22$ at ambient temperature has been stated [3]. Here we report on the synthesis, the crystal structure, the Cu X-ray absorption spectrum, the ion conductivity and the thermoelectric properties of the extraordinarily copper-rich sulfide chloride $Cu_{22}Bi_{12}S_{21}Cl_{16}$.

2. Experimental section

2.1. Synthesis

The starting materials for the synthesis of $Cu_{22}Bi_{12}S_{21}Cl_{16}$ were Cu (Chemapol; p.a.), Bi_2S_3 (Alfa Aesar, 99.9%), S (Laborchemie Apolda; purified und distilled), and CuCl, which was synthesized from $CuSO_4 \cdot 5H_2O$ (Grüssing; p.a.) and NaCl (VWR; p.a.) according to Kramb et al. [4]. In an argon filled glove box (Braun, $c(O_2) \leq 1$ ppm, $c(H_2O) \leq 1$ ppm), a silica ampoule (150 mm in length, 15 mm inner diameter) was loaded with about 1 g of a mixture that corresponds to the product composition. In a tubular furnace, the evacuated ($p \approx 0.1$ Pa) and sealed ampoule was heated to 1120 K, cooled to 670 K with $\Delta T/t=10$ K h^{-1}, further cooled to 570 K with $\Delta T/t=1$ K h^{-1}, and tempered at 570 K for two weeks before quenching in water. The product consisted of black needle-shaped crystals, which are inert to water and alcoholic solvents, but decompose in inorganic acids.

2.2. Thermal analysis

A powdered sample of about 30 mg was sealed in a micro ampoule at $p \approx 0.1$ Pa. The thermal decomposition of $Cu_{22}Bi_{12}S_{21}Cl_{16}$ was analyzed using a DTA-DSC system (Labsys DSC 12, Setaram). With

* Corresponding author. Fax: +49 351 463 37287.
E-mail address: michael.ruck@tu-dresden.de (M. Ruck).

0022-4596/$ - see front matter © 2010 Elsevier Inc. All rights reserved.
doi:10.1016/j.jssc.2010.10.038

a rate of $\Delta T/t = 5\ \mathrm{K\ min^{-1}}$ the samples were heated to 770 K and subsequently cooled to ambient temperature. The residua of the thermal analysis were characterized by X-ray powder diffraction.

2.3. XANES experiments

X-ray absorption near edge spectroscopy was applied to determine the valence of the copper ions in the material. It was performed at the Doris ring at HASYLAB of DESY in Hamburg. The examination took place at the beam line E4 at the Cu–K-edge in the range from 8729 to 9977 eV with a step width of 0.2 eV.

2.4. Thermoelectric measurements

A pressed powder pellet ($2.7 \times 1.65 \times 1.5\ \mathrm{mm^3}$) of $Cu_{22}Bi_{12}S_{21}Cl_{16}$ was analyzed for electrical and thermal conductivity as well as Seebeck coefficient in the temperature range between 5 and 300 K with a step width of about 6 K using a Quantum Design PPMS with thermal transport option. The pellet was contacted with Ag-containing epoxy glue. The measured thermal conductivity includes a material independent contribution of heat radiation, which becomes substantial above 150 K.

2.5. Conductivity measurements

All measurements were performed in dry N_2 atmosphere. The density of the polycrystalline samples (sintered in N_2 at 570 K for 2 d) was about 80%. The total conductivity of polycrystalline samples was obtained from the high-frequency intercept of impedance spectra (Novocontrol High Resolution Dielectric Analyzer) measured with sputtered Pt electrodes. The total conductivity of single crystals was measured by impedance spectroscopy after contacting the crystals with small droplets of $In_{11}Ga_{89}$ alloy (liquid at 298 K) at the ends.

The ionic conductivity for copper ions was determined from DC polarization experiments with electron-blocking electrodes. For this purpose, polycrystalline $Cu_{0.75}Rb_{0.25}Cl$ was used as pure copper ion conducting membrane [5,6]. Its electronic (hole) conductivity is less than $2 \times 10^{-12}\ \mathrm{S\ cm^{-1}}$ below 410 K [5]. $Cu_{0.75}Rb_{0.25}Cl$ pellets were obtained by finely mixing, grinding, and uniaxial pressing of appropriate amounts of CuCl and RbCl in a glove box. To achieve fast Cu exchange kinetics, on one side a mixture of $Cu_{0.75}Rb_{0.25}Cl$ and Cu powder was pressed on the $Cu_{0.75}Rb_{0.25}Cl$ pellets. These composite electrodes were kept for 3 days at 410 K in N_2 to achieve interdiffusion of Cu^+ and Rb^+ within the $Cu_{0.75}Rb_{0.25}Cl$ yielding a good electrolyte. Conductivity, determined by impedance spectroscopy, and activation energy were close to literature data [5,6]. For conductivity measurements, polycrystalline samples were spring-loaded between the composite electrodes with the copper metal side pointing towards copper foils as outer current collectors.

Needle-shaped single-crystals, typically 1.5–2 mm long with 30–40 μm diameter (long axis corresponds to [0 0 1] orientation), were contacted in a home-built micro contact setup (see e.g. [7]) under a microscope. The crystal was placed on a sapphire base plate and pieces of the $Cu_{0.75}Rb_{0.25}Cl$/Cu composite electrodes were arranged over its ends (Cu side up). The Cu top layer of the electrode pellets were contacted by Pt/Ir tips. To achieve good contact between the $Cu_{0.75}Rb_{0.25}Cl$ electrolyte and the crystal, it proved necessary to carefully heat the setup until the $Cu_{0.75}Rb_{0.25}Cl$ was just melted (nominal temperature $T \approx 440$ K), and then to quickly cool below the melting point. Thus, the free part of the crystal between the electrodes was approx. 1 mm. For one crystal this contacting procedure was repeated to perform a second set of measurements, a second crystal was mounted only once. Two-point DC conductivity measurements were performed in galvanostatic mode with a Keithley 2400 SourceMeter. The applied current was chosen such that the voltage drop over the sample typically did not exceed 15 mV.

2.6. Crystallographic structure determination

Powder diffractograms were measured with a Stadi-P diffractometer (Stoe) equipped with a position sensitive detector using Cu–$K\alpha_1$ radiation. Single crystals were examined using Buerger precession method (Zr-filtered Mo radiation, imaging plate technique). Diffraction intensity data were collected on single-crystal diffractometers with imaging plates at 293(2) (IPDS-I, Stoe) and at 150(2) K (IPDS-II, Stoe) using monochromatized Mo–$K\alpha$-radiation. A numerical absorption correction was applied [8] based on a microscopic crystal description that had been optimized using sets of symmetry equivalent reflections [9]. Experimental details are summarized in Table 1.

The crystal structure was solved by direct methods in the space group $P6/m$ (no. 175) and refined against F^2 [10]. During the first steps of the structure solution two Bi and four anion positions were found. Due to the very similar X-ray scattering factors, the assignment of S and Cl atoms to the anion positions is based on bond-length bond-strength considerations (Table S1 of the Supplement) [11]. The position S4/Cl4 was considered to be mixed occupied. Anisotropic displacement parameters were determined for these atoms. Difference Fourier maps showed numerous maxima, which could be assigned to partially occupied Cu positions. Those significant within the bias in the Fourier map were included in the refinement procedure. The sum of occupancies for all disordered Cu atoms was fixed based on charge balance and the assumption of the Cu oxidation state +I. For all Cu atoms the same isotropic displacement parameter was applied. Structure data are listed in Table 2 and in Table S2 of the Supplementary material. Further details of the crystal structure determination are available from the Fachinformationszentrum Karlsruhe, D-76344 Eggenstein-Leopoldshafen (Germany), E-mail: crysdata@fiz-karlsruhe.de, on quoting the depository numbers CSD-421945 (293 K) and CSD-421946 (150 K). For graphical representation of the crystal structure the program Diamond [12] was used.

An alternative description of the electron density at 293(2) K associated with the disordered Cu cations was elaborated based on the anharmonic refinement of two positions with third-order tensors and the harmonic, anisotropic refinement of seven positions (Tables S3 and S4 of the Supplement). In the case of the structure determination at 150 K, four atoms were refined with third-order tensors and five with second-order tensors (Tables S5 and S6). Since these refinements do not show large negative residual electron densities they can be regarded as adequate descriptions of the disorder [13]. The Joint Probability Density Function [13] was calculated with JANA [14] and visualized with VESTA [15]. Selected one-particle-potentials and their errors were determined [13,14].

3. Results and discussion

3.1. Synthesis and valence of copper

The thermal reaction of Cu, CuCl, S, and Bi_2S_3 resulted in black needles of the sulfide chloride $Cu_{22(1)}Bi_{12}S_{21(1)}Cl_{16(1)}$. With respect to the pseudo-ternary phase diagram the sum formula can be rearranged as $4CuCl \cdot 9Cu_2S \cdot 12BiSCl$. Heating $Cu_{22}Bi_{12}S_{21}Cl_{16}$ in evacuated silica ampoules leads to peritectic decomposition at 649(5) K. After cooling to ambient temperature the X-ray powder diffraction detected species were $Cu_{22}Bi_{12}S_{21}Cl_{16}$, $Cu_3Bi_2S_4Cl$ [16], and CuCl.

Table 1
Crystallographic data and information of the structure determinations for $Cu_{22}Bi_{12}S_{21}Cl_{16}$.

Refined composition	$Cu_{22(1)}Bi_{12}S_{21(1)}Cl_{16(1)}$	
Measuring temperature	293(2) K	150(2) K
Crystal system; space group	Hexagonal; *P*6/*m* (no. 175)	
a/pm	2116.7(7)	2108.8(9)
c/pm	395.17(5)	395.13(2)
V/(10^6 pm^3)	1533.3(7)	1521.7(1)
Z	1	
$\rho_{calc.}$/(g cm^{-3})	5.57	5.62
Crystal dimensions/mm^3	0.02 × 0.02 × 0.30	
Measuring system	IPDS-I (Stoe)	IPDS-II (Stoe)
Radiation	Graphite-monochromated Mo-*K*α, λ = 71.073 pm	
Measuring range	$2\theta \le 51.5^\circ$	$2\theta \le 66.7^\circ$
	$-25 \le h, k \le 25$; $-4 \le l \le 4$	$-32 \le h, k \le 32$; $-5 \le l \le 6$
Absorption correction	Numerical; crystal description optimized using sets of symmetry equivalent reflections	
μ(Mo-*K*α) × mm	43.2	43.5
Transmission factors	0.33–0.59	0.06–0.65
Measured, unique reflections	12011, 1112	27425, 2206
R_{int}; R_σ	0.077; 0.033	0.077; 0.027
Structure refinement	Least squares method; full matrix; based on F^2	
Extinction parameter	$5.3(3) \times 10^{-4}$	$1.8(3) \times 10^{-4}$
Parameters; Restrictions	118; 1	131; 1
Residual electron density $\Delta\rho$/(e 10^{-6} pm^{-3})	+1.5 to −1.5	+2.2 to −2.2
R_1 (all F_o)	0.043	0.048
R_1 ($F_o > 4\sigma(F_o)$)	0.031	0.043
wR_2 (all F_o^2)	0.033	0.056

Table 2
Wyckoff positions, coordinates, occupancy factors (*k*) and equivalent/isotropic displacement parameters (/pm^2) of the atoms in $Cu_{22}Bi_{12}S_{21}Cl_{16}$ at 293(2) K and 150(2) K (italic). U_{eq} is defined as one third of the trace of the orthogonalized tensor U_{ij}. The occupancy of the mixed anion position is *k* Cl4 and (1–*k*) S4.

Atom	Pos.	*x*		*y*		*z*		*k*		U_{eq},U_{iso}	
Bi1	6*k*	0.24744(2)	*0.24679(2)*	0.18663(2)	*0.18647(2)*	1/2	*1/2*	1	*1*	203(1)	*171.1(8)*
Bi2	6*k*	0.56226(2)	*0.56203(2)*	0.17680(2)	*0.17689(2)*	1/2	*1/2*	1	*1*	151(1)	*119.6(7)*
Cu1	6*j*	0.062(4)	*0.069(1)*	0.054(7)	*0.048(1)*	0	*0*	0.0765(7)	*0.075(6)*	197(5)	*147(3)*
Cu2	6*j*	0.066(3)	*0.060(1)*	0.03(1)	*−0.002(1)*	0	*0*	0.052(8)	*0.081(8)*	U_{iso}(Cu1)	U_{iso}(*Cu1*)
Cu3	12*l*	0.075(1)	*0.0750(8)*	0.063(1)	*0.0628(7)*	0.109(7)	*0.128(5)*	0.064(5)	*0.055(3)*	U_{iso}(Cu1)	U_{iso}(*Cu1*)
Cu4	6*j*	0.355(1)	*0.3578(3)*	0.099(1)	*0.1008(5)*	0	*0*	0.34(4)	*0.42(2)*	U_{iso}(Cu1)	U_{iso}(*Cu1*)
Cu5	6*j*	0.372(2)	*0.371(1)*	0.121(2)	*0.122(1)*	0	*0*	0.36(2)	*0.24(1)*	U_{iso}(Cu1)	U_{iso}(*Cu1*)
Cu6	6*j*	0.3896(7)	*0.3876(4)*	0.150(1)	*0.1473(5)*	0	*0*	0.27(2)	*0.30(1)*	U_{iso}(Cu1)	U_{iso}(*Cu1*)
Cu7	6*j*	0.435(2)	*0.431(3)*	0.205(3)	*0.200(3)*	0	*0*	0.044(6)	*0.021(3)*	U_{iso}(Cu1)	U_{iso}(*Cu1*)
Cu8	6*j*	0.4300(9)	*0.4321(6)*	0.230(1)	*0.2301(7)*	0	*0*	0.089(7)	*0.100(4)*	U_{iso}(Cu1)	U_{iso}(*Cu1*)
Cu9	6*j*	0.4264(6)	*0.4242(8)*	0.276(1)	*0.2694(9)*	0	*0*	0.119(5)	*0.074(4)*	U_{iso}(Cu1)	U_{iso}(*Cu1*)
Cu10	12*l*	0.445(1)	*0.4478(9)*	0.270(1)	*0.2761(7)*	0.26(1)	*0.331(7)*	0.057(7)	*0.09(1)*	U_{iso}(Cu1)	U_{iso}(*Cu1*)
Cu11	12*l*	0.4473(4)	*0.4467(7)*	0.2797(3)	*0.2803(4)*	0.404(3)	*0.415(5)*	0.255(8)	*0.17(1)*	U_{iso}(Cu1)	U_{iso}(*Cu1*)
Cu12	6*k*	0.4274(9)	*0.432(1)*	0.2834(5)	*0.2822(5)*	1/2	*1/2*	0.165(9)	*0.13(1)*	U_{iso}(Cu1)	U_{iso}(*Cu1*)
Cu13	12*l*	0.4283(7)	*0.4270(6)*	0.2862(6)	*0.2842(6)*	0.270(4)	*0.143(3)*	0.101(4)	*0.067(2)*	U_{iso}(Cu1)	U_{iso}(*Cu1*)
Cu14	6*j*	0.4332(8)	*0.4341(5)*	0.311(2)	*0.3089(6)*	0	*0*	0.093(5)	*0.115(3)*	U_{iso}(Cu1)	U_{iso}(*Cu1*)
Cu15	6*j*	0.4269(4)	*0.4274(5)*	0.3558(6)	*0.3527(8)*	0	*0*	0.210(5)	*0.146(9)*	U_{iso}(Cu1)	U_{iso}(*Cu1*)
Cu16	6*j*	0.4238(9)	*0.4245(7)*	0.390(2)	*0.371(1)*	0	*0*	0.14(1)	*0.092(8)*	U_{iso}(Cu1)	U_{iso}(*Cu1*)
Cu17	6*j*	0.4382(7)	*0.4310(5)*	0.421(1)	*0.4096(8)*	0	*0*	0.51(1)	*0.28(1)*	U_{iso}(Cu1)	U_{iso}(*Cu1*)
Cu18	6*j*	0.458(2)	*0.4457(4)*	0.447(2)	*0.4305(5)*	0	*0*	0.14(2)	*0.48(1)*	U_{iso}(Cu1)	U_{iso}(*Cu1*)
Cu19	6*i*	1/2	*1/2*	1/2	*1/2*	0.128(8)	*0.132(6)*	0.053(4)	*0.047(3)*	U_{iso}(Cu1)	U_{iso}(*Cu1*)
Cu20	12*l*	0.4666(9)	*0.468(1)*	0.4835(8)	*0.4849(9)*	0.277(5)	*0.271(5)*	0.060(2)	*0.041(2)*	U_{iso}(Cu1)	U_{iso}(*Cu1*)
Cu21	6*k*	–	*0.345(4)*	–	*0.073(4)*	–	*1/2*	–	*0.013(3)*	–	U_{iso}(*Cu1*)
Cu22	6*j*	–	*0.306(3)*	–	*0.089(3)*	–	*0*	–	*0.017(3)*	–	U_{iso}(*Cu1*)
Cu23	12*l*	–	*0.4340(6)*	–	*0.2833(5)*	–	*0.346(3)*	–	*0.123(7)*	–	U_{iso}(*Cu1*)
Cu24	6*j*	–	*0.468(2)*	–	*0.461(2)*	–	*0*	–	*0.050(5)*	–	U_{iso}(*Cu1*)
S1	6*k*	0.3577(1)	*0.3572(1)*	0.1665(1)	*0.1660(1)*	1/2	*1/2*	1	*1*	153(6)	*137(3)*
S2	6*j*	0.4709(1)	*0.4704(1)*	0.1047(1)	*0.1049(1)*	0	*0*	1	*1*	141(6)	*120(3)*
S3	6*k*	0.6011(1)	*0.6009(1)*	0.0800(1)	*0.0797(1)*	1/2	*1/2*	1	*1*	163(6)	*126(3)*
Cl4/S4	6*j*	0.3101(1)	*0.3104(1)*	0.2862(1)	*0.2861(1)*	0	*0*	0.42(1)	*0.40(1)*	192(10)	*162(6)*
Cl1	1*b*	0	*0*	0	*0*	1/2	*1/2*	1	*1*	428(23)	*385(15)*
Cl2	6*j*	0.1863(1)	*0.1861(1)*	0.0698(1)	*0.0692(1)*	0	*0*	1	*1*	222(7)	*182(4)*
Cl3	6*j*	0.5490(2)	*0.5480(1)*	0.3031(2)	*0.3029(1)*	0	*0*	1	*1*	270(8)	*204(4)*

Oxidation state +I of the copper cations was verified by XANES measurements (Fig. 1). The energy of the copper *K* edge of $Cu_{22}Bi_{12}S_{21}Cl_{16}$ is very similar to the reference CuCl, while there is a large difference to the position of the edge of CuS. The suppression of the distinct maximum at the boundary of the absorption edge on the higher energy side (white-line) in the X-ray absorption spectrum of $Cu_{22}Bi_{12}S_{21}Cl_{16}$ can be interpreted as a hint to a predominantly covalent character of the copper–ligand bond [17].

3.2. Crystal structure

$Cu_{22(1)}Bi_{12(1)}S_{21(1)}Cl_{16(1)}$ crystallizes in the hexagonal space group $P6/m$ with $Z=1$ and cell parameters $a=2116.7(7)$ pm, $c=395.17(5)$ pm at 293(2) K. The structural changes upon cooling to 150 K are marginal and affect mainly the Cu atoms. The crystal structure can be subdivided into rigid coordination networks formed by the bismuth cations and the anions, and more or less mobile Cu cations in between (Fig. 2).

Each of the two independent bismuth cations is coordinated by three sulfide and four chloride anions in the shape of a mono-capped trigonal prism. Such coordination of bismuth cations has already been reported for $Cu_3Bi_2S_4Cl$ [16], $Cu_7Bi_6S_{10}Cl_5$ [2], and $Cu_9Bi_9S_{16}Cl_8$ [1]. The $[BiS_3Cl_4]$ polyhedra share their trigonal faces to form rods parallel [0 0 1]. By sharing those edges that are defined by chloride anions the prism rods constitute tubes $[BiS_{1/1}S_{2/2}Cl^{2-}_{4/4}]_n$ with hexagonal ($n=6$) and trigonal ($n=3$) cross-sections. The hexagonal tube is filled with chloride ions, which are placed on the central axis, and copper cations, which are largely disordered. Tubes of this kind have previously been found in the structure of $Cu_{7.4}Bi_6Se_{12}Cl_7$ and have been discussed there comprehensively [1].

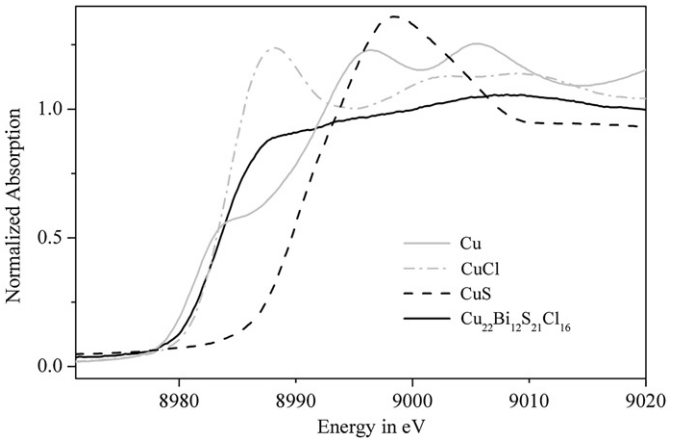

Fig. 1. XANES spectrum at the Cu K edge of $Cu_{22}Bi_{12}S_{21}Cl_{16}$ as well as of reference substances.

One of the sulfide ions that form the outer surface of the hexagonal tube is partially substituted by chloride (Wyckoff site 6*j*). This opens the way to a phase width of the compound, which is yet undetermined, but could in principle range from the copper-rich $Cu_{25}Bi_{12}S_{24}Cl_{13}$ ($=CuCl\cdot 12Cu_2S\cdot 12BiSCl$) to the copper-poorer $Cu_{19}Bi_{12}S_{18}Cl_{19}$ ($=7CuCl\cdot 6Cu_2S\cdot 12BiSCl$). For many mixed conductors, a composition variation within the possible phase width will affect the electronic conductivity more than the ion transport.

The 1.5 ± 0.1 copper ions per unit cell (i.e. formula unit) inside the hexagonal tubes are spread over the positions Cu1 to Cu3 (24 sites per unit cell), which form a torus around the *c* axis. There might be a local cation mobility in the torus, but ion exchange between them seems to be unlikely (inter-torus distance 309 pm).

The majority of the copper cations (about 21 ± 1 Cu per formula unit) is distributed over numerous sites between the tubes (at 293 K 126 sites per unit cell). The analysis of scenarios of simultaneous occupancies of sites between the tubes reveals that 21 copper cations per unit is yet the highest possible filling degree. The coordination of the copper cations is trigonal or tetrahedral and dominated by sulfide ions. In the projection on the (0 0 1) plane these positions form snake-like ensembles, which are clearly separated from each other. Along the [0 0 1] direction the "snakes" proof to be interconnected by partially occupied sites, denoted as Cu10 to Cu13 (Fig. 3). Cu9 is at the intersection of Cu diffusion paths parallel and perpendicular to the *c*-axis.

Instead of 17 copper positions with an isotropic displacement parameter, eight positions with harmonic and anharmonic tensors can be used to describe the electron density. In the thereof derived Joint Probability Density Function (JPDF) these diffusion paths are even more evident. If the string of positions along [0 0 1] is

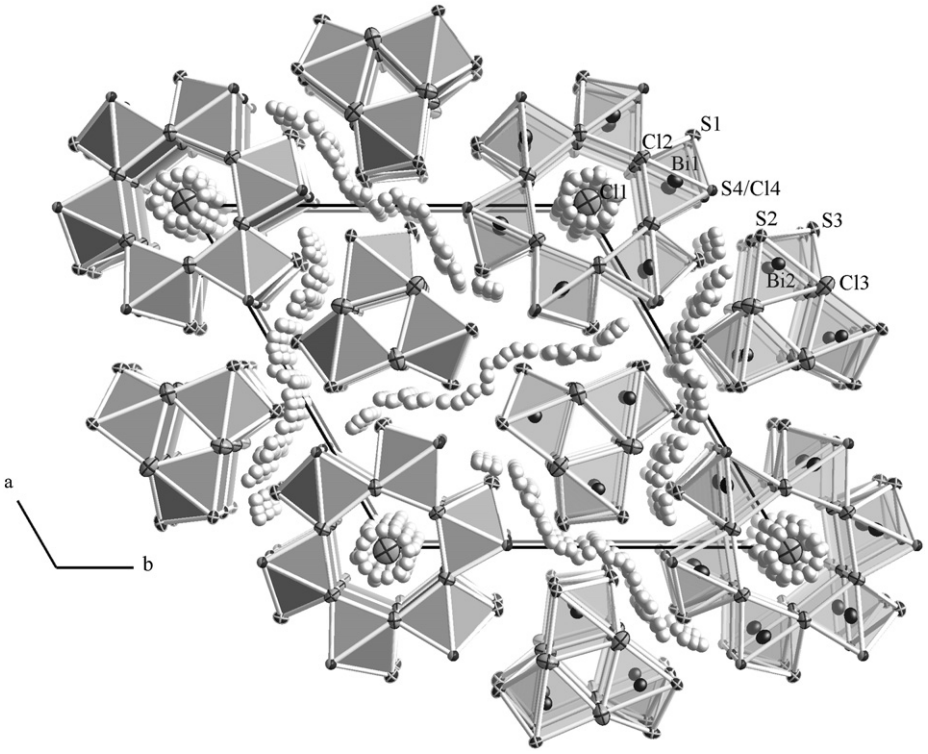

Fig. 2. Projection of the crystal structure of $Cu_{22}Bi_{12}S_{21}Cl_{16}$ along [0 0 1]. Cu atoms are represented by white ellipsoids. The ellipsoids cover 95% probability.

regarded as the "street" for mobile copper cations, the side positions are the "parking". Very similar to the situation in $Cu_7Bi_6S_{10}Cl_5$ [2], the parking sites in the dead ends, formed by the closely spaced positions Cu4 to Cu8, are fully occupied in total. With respect to fast ion conductivity in a pseudo one-dimensional system this is an unwanted situation. Fortunately, the middle parts, i.e. the "steps of the ladder", provide the possibility for easy exchange of cations and thus allows for a redirection to another "street" in case one channel should be blocked. Only in about 50% of all cases the Cu17 position is occupied and blocks the positions Cu14 and Cu15. If one of the positions Cu18 to Cu20 is occupied, a side-step of a cation moving along [0 0 1] becomes feasible.

In order to estimate the mobility of copper cations along the path, pseudo-potentials $V(x)$ [13,18] were derived from the probability density function pdf(x) at 150 K using the relation $V(x)=V_0-kT\ln[\mathrm{pdf}(x)]$. The calculated hopping barriers are quite small, about 37 meV only (Fig. 4), yet, the effective potential could be substantially higher [13]. $Ag_{1-x}[W_2O_2Cl_6]$, whose local silver disorder is related to the present one, exhibits pseudo-potentials of 13 meV calculated with the same method [19].

3.3. Ionic conductivity

The impedance spectrum of the $Cu_{22}Bi_{12}S_{21}Cl_{16}$ single-crystal (Fig. 5) illustrates the electrical properties of the material. It contains a high-frequency axis intercept corresponding to the total bulk conductivity of the sample. At lower frequency it is followed by a deformed semicircle extending to very low frequencies (6×10^{-3} Hz) due to the stoichiometry polarization in the sample, caused by the Cu^+-conducting but electron-blocking $Cu_{0.75}Rb_{0.25}Cl$ electrodes, when approaching the DC limit. The respective resistance yields the ionic part of the conductivity. As the impedance spectra become rather noisy when moving to lower temperatures, the ionic conductivity was instead determined from DC experiments with electron-blocking electrodes in the arrangement $Cu/Cu_{0.75}Rb_{0.25}Cl/Cu_{22}Bi_{12}S_{21}Cl_{16}/Cu_{0.75}Rb_{0.25}Cl/Cu$ (due to its large area compared to the single-crystal sample, the exchange reaction $Cu \Leftrightarrow Cu^+ + e^-$ at the Cu current collector can be regarded as reversible).

Fig. 6 shows a typical DC polarization experiment on a single-crystal. Since the $Cu_{0.75}Rb_{0.25}Cl$ electrodes only allow ions to pass, the voltage under steady-state conditions corresponds to the ionic conductivity of the sample. The resulting ionic conductivity values σ_{ion} along the crystallographic [0 0 1] direction are collected in Fig. 7. The agreement between the three individual measurement series is good. The ionic conductivity at 450 K is about $\sigma_{ion}=0.06$ S cm^{-1}, i.e. comes near superionic materials such as $RbAg_4I_5$ (0.7 S cm^{-1} at 450 K) or α-AgI (1.5 S cm^{-1} at 450 K) [20]. From an Arrhenius plot of $\sigma_{ion}\cdot T$ versus T^{-1}, the activation energy for Cu^+ ionic conduction along [0 0 1] is determined as $E_a=0.44$ eV. At high temperature, the ionic conductivity of the $Cu_{22}Bi_{12}S_{21}Cl_{16}$ single-crystals exceeds that of the $Cu_{0.75}Rb_{0.25}Cl$ electrolyte. Fortunately, the geometry of the experiment – crystal diameter 30–40 μm but diameter of the composite electrode pellets about 2 mm – ensured that the electrolyte's contribution to the total DC resistance is negligible. The electronic conductivity is higher than σ_{ion} by a factor of 4–300 in the temperature range studied, making it a mixed conductor. The activation energy of σ_{eon} is below 0.1 eV (vide infra).

While the steady-state voltage drop yields the conductivity of the non-blocked carrier (here: Cu^+ ions), from the sloping transient behavior after switching on or off the current, the chemical diffusion coefficient of copper D^{δ}_{Cu} can be obtained from a plot of

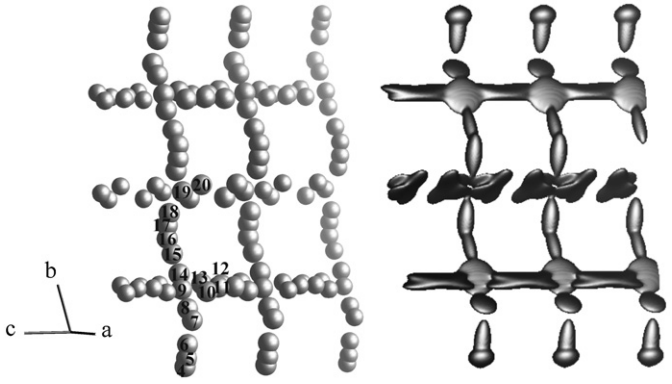

Fig. 3. Distribution of the copper(I) cations between the polyhedral tubes at 293 K, described with 17 unique split positions with the same isotropic displacement parameter (left) or, alternatively, as JPDF (isosurface level $\eta=0.08$ e/(10^6 pm^3)) of eight harmonically or anharmonically refined positions (right).

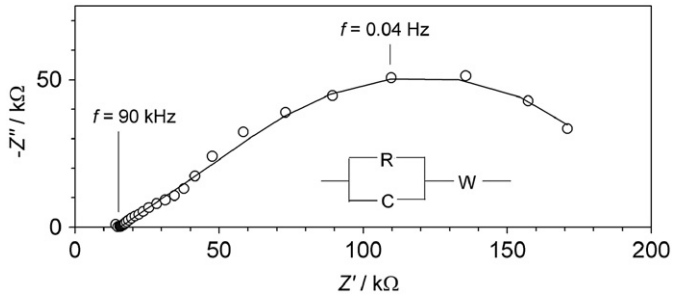

Fig. 5. Impedance spectrum of the first single-crystal, second contacting, with electron-blocking $Cu/Cu_{0.75}Rb_{0.25}Cl/Cu_{22}Bi_{12}S_{21}Cl_{16}/Cu_{0.75}Rb_{0.25}Cl/Cu$ electrodes at 430 K. The line represents a fit with the equivalent circuit shown as inset. R, C are bulk resistance and capacitance; W designates a "Warburg" element.

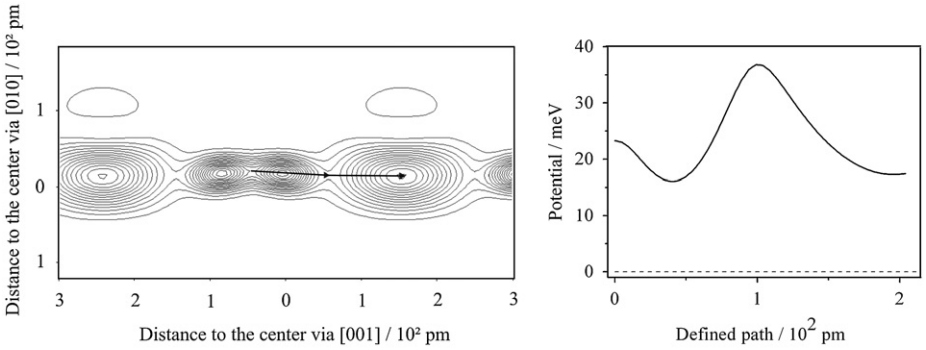

Fig. 4. JPDF of Cu2″ and Cu7″ (harmonically refined; 150 K) and resulting potentials (solid) and errors (dashed) along the defined path at section $x=0.4253$. Contour intervals are 0.08 e · 10^{-6} pm^{-3}.

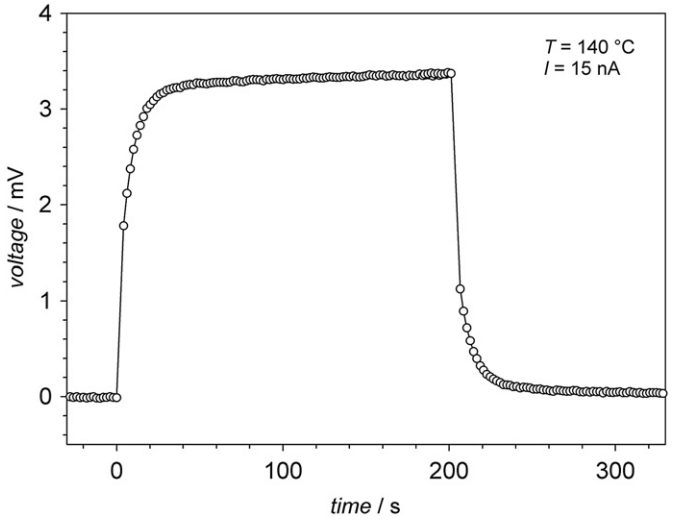

Fig. 6. DC polarization measurement of a $Cu_{22}Bi_{12}S_{21}Cl_{16}$ single-crystal with electron-blocking $Cu_{0.75}Rb_{0.25}Cl$ electrodes. A current of 15 nA was drawn for 200 s.

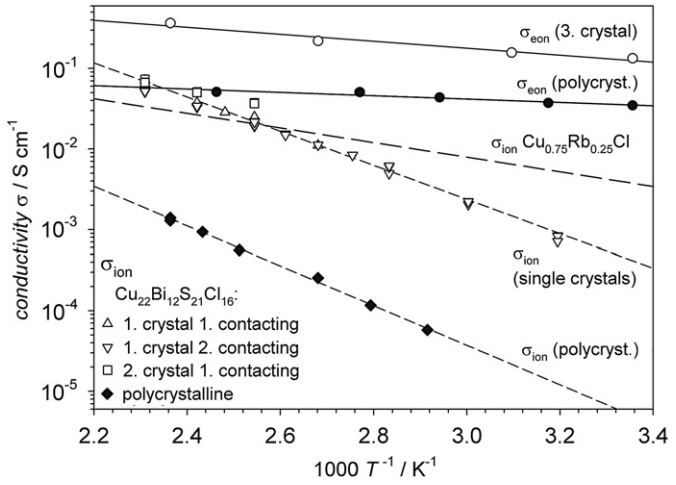

Fig. 7. Cu^+ ionic conductivity of $Cu_{22}Bi_{12}S_{21}Cl_{16}$ single-crystals along [0 0 1] (open symbols) and polycrystalline samples (solid symbols). For comparison, also the electronic conductivity as well as the ionic conductivity of $Cu_{0.75}Rb_{0.25}Cl$ are shown.

$\ln[U_\infty - U(t)]$ versus t [21–23]. Fig. 8 shows the chemical diffusion coefficient of copper D^δ_{Cu} obtained from the polarization transients of the single-crystals, having an activation energy of $E_a = 0.25(5)$ eV. The chemical diffusion coefficient in a mixed conductor with $\sigma_{eon} > \sigma_{ion}$ can be expressed as

$$D^\delta_{Cu} = \frac{RT}{F^2}\sigma_{ion}\left(\frac{\chi_{ion}}{c_{ion}} + \frac{\chi_{eon}}{c_{eon}}\right)$$

with F is the Faraday constant, and χ_{eon}, χ_{ion} are trapping factors ("trapping" could occur e.g. by holes being small polarons, or interactions of negative defects such as copper vacancies with positive defects) [23].

Lacking further information, we have to make some approximations when trying to analyze the measured D^δ_{Cu} values in order to get first insights into the material's defect chemistry. Neglecting trapping reactions ($\chi_{eon}, \chi_{ion} \approx 1$) and assuming $c_{eon} \geq c_{ion}$ (justified by the most probable electroneutrality condition of copper vacancies being compensated by electron holes), the equation reduces to $D^\delta_{Cu} \approx D_{Cu+}$ [23]. Then the mobile ion concentration can be estimated using the Nernst–Einstein equation. It increases from about 10^{18} at 310 K to 10^{19} cm^{-3} at 420 K (a concentration of 10^{19} cm^{-3} corresponds to 0.07% of the copper cations).

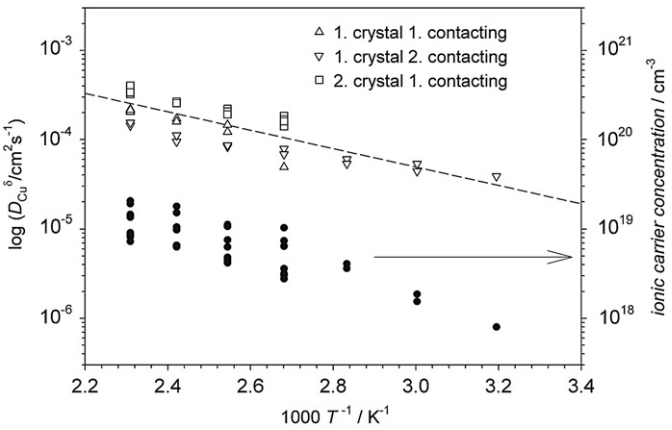

Fig. 8. Chemical diffusion coefficient of copper D^δ_{Cu} in $Cu_{22}Bi_{12}S_{21}Cl_{16}$ single-crystals determined from the transients in DC polarization curves. Solid symbols: concentration of mobile ionic carriers calculated from D_{Cu+} and σ_{ion} by the Nernst–Einstein equation.

A certain contribution of σ_{ion}/c_{eon} to D^δ_{Cu} will lead to an overestimation of D_{Cu+} and thus the obtained ionic charge carrier concentration (Fig. 8) is a lower limit. Also its apparent temperature dependence has to be regarded with some care since it may be affected by a σ_{ion}/c_{eon} contribution.

The observation, that the ionic charge carrier concentration is significantly lower than the concentration of regular copper ions, points towards copper vacancies being the mobile ionic species. There are equally probable charge compensation mechanisms for negatively charged copper vacancies, which cannot be distinguished within this study: (i) some Cu^{2+} on Cu^+ sites (=electron holes), (ii) S^- on S^{2-} sites, or (iii) some Cl^- on S^{2-} sites (slight stoichiometry deviation). P-type electronic conductivity is indeed observed (see below), and this also disfavors the alternative hypothesis of copper interstitials being the mobile copper species.

Fig. 9 shows SEM pictures of a polycrystalline sample. The relative sample density of about 80% indicates a very early stage of sintering, and the large porosity visible in Fig. 9 confirms this. The primary crystallites are needle-shaped with a diameter of about 0.1 μm and a length of 0.5 μm up to several μm. While on a short range scale parallel bundles of crystallites can be recognized, at a larger scale no texture is observed. The connection between individual crystallites or crystallite bundles seems to be restricted to rather small contact areas.

Compared to the single-crystals, the ionic conductivity of the porous $Cu_{22}Bi_{12}S_{21}Cl_{16}$ pellet is lower by more than one order of magnitude, and the activation energy is slightly higher ($E_a = 0.51$ eV). This can be due to several individual or combined reasons:

(i) Current constriction effects caused by small crystal-to-crystal contact area probably represent the largest contribution. Since the difference in σ_{eon} between pellet and single-crystal is smaller, poor connectivity cannot completely explain the higher σ_{ion} for single-crystals.
(ii) Impeded ion transport through grain boundaries: there is no direct evidence from impedance spectra of polycrystalline samples, but they are too complex to completely rule out grain boundary effects.
(iii) Largely anisotropic Cu^+ conductivity attributable to the crystal structure: the actual impact of this anisotropy on the pellet conductivity sensitively depends on the microstructure details.

For comparison: Cold pressed powder pellets of $(CuI)_2Cu_3SbS_3$ and $(CuI)_3Cu_2TeS_3$, which exhibit also anisotropic copper conductivity, showed values of $E_a = 0.35$ eV and $\sigma_{ion} = 1.9 \times 10^{-3}$ S cm^{-1}

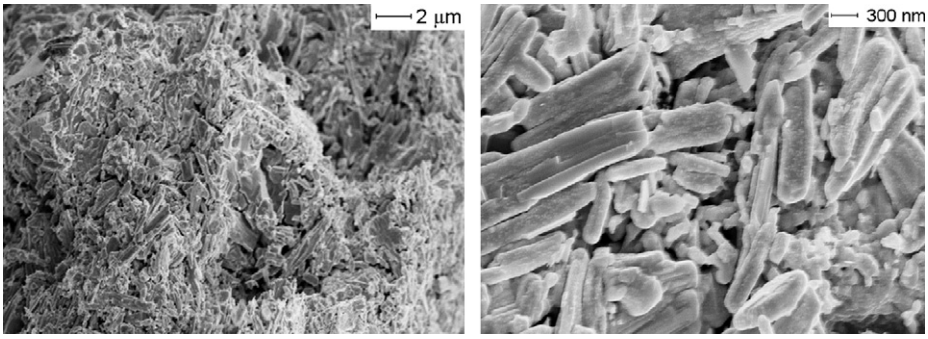

Fig. 9. SEM images of the sintered pellet. Despite needle-shaped crystallites and uniaxial pressing no pronounced texture on long-range scale was observed.

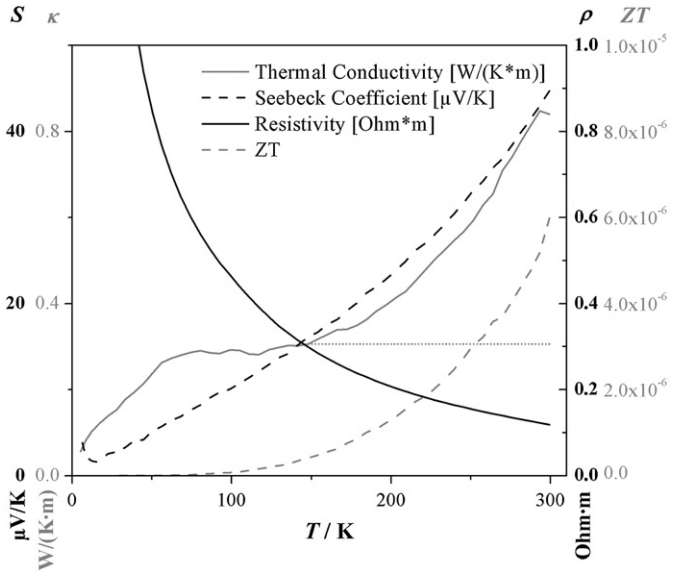

Fig. 10. Electrical resistivity, Seebeck coefficient, thermal conductivity and resulting *ZT* of a pressed pellet of $Cu_{22}Bi_{12}S_{21}Cl_{16}$.

(470 K) resp. $E_a=0.2$ eV and $\sigma_{ion}=3\times10^{-3}$ S cm^{-1} (470 K) [24]. One should note that the $Cu_{22}Bi_{12}S_{21}Cl_{16}$ single-crystals do not only show a high Cu^+ conductivity, but also a high chemical diffusivity for copper as well as ambipolar conductivity, which are important properties of good electrode materials.

3.4. Thermoelectric properties

The total electrical resistivity of a powder pellet of $Cu_{22}Bi_{12}S_{21}Cl_{16}$ exhibits semiconducting behavior in the temperature range between 5 and 300 K. The band gap that was derived from the electrical resistivity varies between 0.01 eV in the extrinsic regime and 0.1 eV in the intrinsic regime. The optical band gap seems to be much wider since the optical absorption of $Cu_{22}Bi_{12}S_{21}Cl_{16}$ increases significantly only above 1.1 eV (see Supplementary material). These observations suggest a highly doped semiconductor with indirect band gap.

Despite the narrow band gap the specific electrical conductivity is rather low ($\sigma=0.081$ S cm^{-1} at 300 K), which seems to result from a low charge carrier concentration or mobility. Assuming that the bands close to the Fermi level are non-degenerated and that the scattering of carriers (r_p) is dominated by structure defects (disorder), the carrier (hole) concentration n_p can be estimated using the relation [25]

$$n_p = 2\exp\left(-\frac{F}{R}S\right)\left(\frac{2\pi m_p^* k_B T}{h^2}\right)^{3/2}\exp\left(\frac{5}{2}\right)\exp(r_p)$$

with effective mass of a light hole $m_p^*;=0.195\ m_e$ [26], $r_p=1.5$, and Seebeck coefficient $S=43$ µV K^{-1}. At 300 K the rather high carrier concentration $n_p=5\times10^{21}$ cm^{-3} results. Consequently the mobility is only $\mu_p=\sigma/(n_p\cdot e)=1\times10^{-4}$ cm^2 V^{-1} s^{-1}.

The positive sign of the Seebeck coefficient indicates the electronic conductivity is due to the migration of electron holes, which – chemically speaking – corresponds to a minute quantity of Cu^{2+} or S^-. The Seebeck coefficient, which enters squared in the *ZT* formula, amounts to $S=43$ µV K^{-1}. Compared to good thermoelectric materials like $AgPb_mSn_nSbTe_{2+m+n}$ with $S=160$ µV K^{-1} [27], the value is too small. The extrapolated thermal conductivity of about $\kappa=0.3$ W K^{-1} m^{-1} is situated in the range of materials like LAST18 [27], which are good thermoelectric materials with low thermal conductivities. The quintessence of that is the very small $ZT=5.2\times10^{-6}$ of $Cu_{22}Bi_{12}S_{21}Cl_{16}$ at 293 K (Fig. 10). The corresponding value for Bi_2Te_3 at room temperature equals one.

4. Conclusion

$Cu_{22}Bi_{12}S_{21}Cl_{16}$ exhibits a promising crystal structure consisting of a rigid tubular skeleton with mobile copper cations in between. Continuous paths for copper(I) cations along [0 0 1] in conjunction with the enhanced ionic conductivity of single-crystals compared to pressed pellets indicate one-dimensional copper ion conductivity. At 450 K respectable values for ion conductivity of about $\sigma_{ion}=6\times10^{-2}$ S cm^{-1} with an activation energy $E_a=0.4$ eV were found for single-crystals parallel to [0 0 1]. High ion conductivity, high chemical diffusivity for copper, and ambipolar conductivity are important properties of a good electrode material. Because of the low electronic conductivity, probably originating from low charge carrier mobility, a thermoelectric application is not reasonable. Other bottlenecks are the peritectic decomposition and the needle-like habitus of the crystals.

Acknowledgments

We thank Mrs. Gudrun Kadner and Mrs. Jutta Krug for their support in the laboratory. Dr. Frauke Phillip helped us in executing and interpreting the XANES experiments. Dr. Walter Schnelle and Mr. Ralf Koban (Max Planck Institute for Chemical Physics of Solids, Dresden) are gratefully acknowledged for the measurement of the thermoelectric parameters.

Appendix A. Supporting material

Supplementary data associated with this article can be found in the online version at doi:10.1016/j.jssc.2010.10.038.

References

[1] A. Heerwig, M. Ruck, Z. Anorg. Allg. Chem. 635 (2009) 2162.
[2] A. Heerwig, M. Ruck, Z. Anorg. Allg. Chem. 636 (2010) 1860.
[3] T. Kyratsi, E. Hatzikraniotis, K.M. Paraskevopoulos, C.D. Malliakas, J.S. Dyck, C. Uher, M.G. Kanatzidis, J. Appl. Phys. 100 (2006) 123704.
[4] V. Kramb, W. Proske, V. Wiskamp, Naturwiss. Unterr.—Chemie 7 (1996) 9.
[5] T. Matsui, J.B. Wagner, J. Electrochem. Soc. 124 (1977) 941.
[6] R. Kanno, Y. Takeda, Y. Masuyama, O. Yamamoto, T. Takahashi, Solid State Ionics 11 (1983) 221.
[7] F.S. Baumann, J. Fleig, G. Cristiani, B. Stuhlhofer, H.-U. Habermeier, J. Maier, J. Electrochem. Soc. 154 (2007) B931.
[8] X-RED32, Data Reduction Program, Version 1.01, Stoe & Cie GmbH, Darmstadt 2001.
[9] X-SHAPE, Crystal Optimisation for Numerical Absorption Correction Program, Version 1.06, Stoe & Cie GmbH, Darmstadt 1999.
[10] (a) G.M. Sheldrick, SHELX97, Programs for crystal structure determination, Univ. Göttingen, 1997;
(b) G.M. Sheldrick, Acta Crystallogr. A64 (2008) 112.
[11] N.E. Brese, M. O'Keeffe, Acta Crystallogr. B47 (1991) 192.
[12] K. Brandenburg, Diamond 3.2e, Crystal and Molecular Structure Visualization, Crystal Impact GbR, Bonn, Germany 2010.
[13] R. Bachmann, H. Schulz, Acta Crystallogr. A40 (1984) 668.
[14] (a) V. Petříček, M. Dušek, L. Palatinus, Jana2000/2006, the crystallographic computing system, Institute of Physics, Praha, Czech Republic, 2009;
(b) V. Petříček, V.A. van der Lee, M. Evain, Acta Crystallogr. A51 (1995) 529;
(c) L. Palatinus, G. Chapuis, J. Appl. Crystallogr. 40 (2007) 786.
[15] K. Momma, F. Izumi, J. Appl. Crystallogr. 41 (2008) 653.
[16] J. Lewis, V. Kupčík, Acta Crystallogr. B30 (1974) 848.
[17] N.N. Saxena, J. Phys. C: Solid State Phys. 8 (1975) 1450.
[18] R. Bachmann, K.D. Kreuer, A. Rabenau, H. Schulz, Acta Crystallogr. B38 (1982) 2361.
[19] J. Beck, W. Hoffbauer, C. Kusterer, M. Schieweling, Z. Anorg. Allg. Chem. 636 (2010) 1827.
[20] S. Chandra, Superionic Solids, North-Holland, Amsterdam, 1981.
[21] C. Wagner, in: Proceedings of the Seventh Meeting of the International Committee on Electrochemical Thermodynamics and Kinetics, Butterworths, London, 1957.
[22] I. Yokata, J. Phys. Soc. Jpn. 16 (1961) 2213.
[23] J. Maier, J. Am. Ceram. Soc. 76 (1993) 76, 1212; 1218; 1223.
[24] A. Pfitzner, S. Reiser, T. Nilges, W. Kockelmann, J. Solid State Chem. 147 (1999) 170.
[25] C. Korte, J. Janek, J. Phys. Chem. Solids 58 (1997) 623.
[26] A. Rubio-Ponce, D. Olguín, I. Hernández-Calderón, Superficies Vacío 16 (2003) 26.
[27] J.R. Sootsman, D.Y. Chung, M.G. Kanatzidis, Angew. Chem. 121 (2009) 8768; J.R. Sootsman, D.Y. Chung, M.G. Kanatzidis, Angew. Chem. Int. Ed. 48 (2009) 8616.